

Orbital motions in the Dark Matter and MOND/MOG scenarios

L. Iorio

*INFN-Sezione di Pisa. Address for correspondence: Viale Unità di Italia 68
70125 Bari, Italy*

tel./fax 0039 080 5443144

e-mail: lorenzo.iorio@libero.it

Abstract

What the outer regions ($r > 20$ kpc) of a typical spiral disk galaxy like, e.g., our Milky Way would look like if the Modified Newtonian Dynamics (MOND) framework was valid? Is, at least in principle, possible to discriminate between MOND and the Cold Dark Matter (CDM) paradigm in such remote peripheries of the Galaxy? These are the questions we try to preliminarily address here. We, first, obtained an effective mass density profile accounting for the DM content of the Galaxy which was able to correctly reproduce its observed velocity rotation curve. Then, we numerically integrated the equations of motion of test particles acted upon by the resulting DM acceleration at several kpc (25-35 kpc and 50-70 kpc). Second, we numerically integrated the MOND-type modified equations of motion of test particles orbiting at the same distances from a localized central body with approximately the same mass of the electromagnetically-detected part of a typical galaxy ($M \approx 6.5 \times 10^{10} M_{\odot}$ for the Milky Way). By using initial conditions corresponding to co-planar trajectories and observed non-Keplerian velocities, we find that, contrary to DM, MOND does not allow for circular orbits yielding, instead, characteristic and quite different orbital patterns. The same holds also for the Yukawa-type Modified Gravity (MOG) scheme recently proposed by Moffat; it yields trajectories rather similar to the MONDian ones. Going out of the galactic plane, we also repeated our analysis for the Small Magellanic Cloud (SMC) at 59 kpc from the center of the Milky Way finding quite different orbital configurations between DM and MOND/MOG.

Keywords: Modified theories of gravity; Characteristics and properties of the Milky Way galaxy

1 Introduction

In many astrophysical systems like, e.g., spiral galaxies and clusters of galaxies a discrepancy between the observed kinematics of their exterior parts and the predicted one on the basis of the Newtonian dynamics and the matter detected from the emitted electromagnetic radiation (visible stars and gas clouds) was present since the pioneering studies by Zwicky (he postulated the existence of undetected, baryonic matter; today, it is believed that the hidden mass is constituted by non-baryonic particles) on the Coma cluster [1], and by Bosma [2] and Rubin and coworkers [5] on spiral galaxies. More precisely, such an effect shows up in the galactic velocity rotation curves [3, 4] whose typical pattern after a few kpc from the center differs from the Keplerian $1/\sqrt{r}$ fall-off expected from the usual dynamics applied to the electromagnetically-observed matter.

As a possible solution of this puzzle, the existence of non-baryonic, weakly-interacting Cold Dark (in the sense that its existence is indirectly inferred only from its gravitational action, not from emitted electromagnetic radiation) Matter (CDM) was proposed to reconcile the predictions with the observations [6] in the framework of the standard gravitational physics; for a general review on the DM issue see, e.g, [7], while for the distribution of DM in galaxies, see, e.g., [8]. To be more definite, let us suppose that a galaxy is embedded in a spherically symmetric dark halo so that its effective density is $\rho = \rho(r)$. The induced gravitational potential U must obey the usual Poisson equation

$$\nabla^2 U = 4\pi G\rho. \quad (1)$$

A choice for ρ which gives satisfactorily results is

$$\rho = \rho_0 \left(\frac{L}{r}\right)^4 \exp\left(-\frac{L}{r}\right), \quad (2)$$

where L is a scale length; the resulting potential is

$$U = 4\pi G\rho_0 L^2 \exp\left(-\frac{L}{r}\right) \quad (3)$$

which yields a radial acceleration

$$A = -\nabla U = -\frac{4\pi G\rho_0 L^3}{r^2} \exp\left(-\frac{L}{r}\right). \quad (4)$$

Thus, by assuming circular trajectories described with orbital frequencies Ω , the non-Keplerian (NK) rotation velocity can be straightforwardly obtained by equating the centripetal acceleration $\Omega^2 r$ to the force per unit

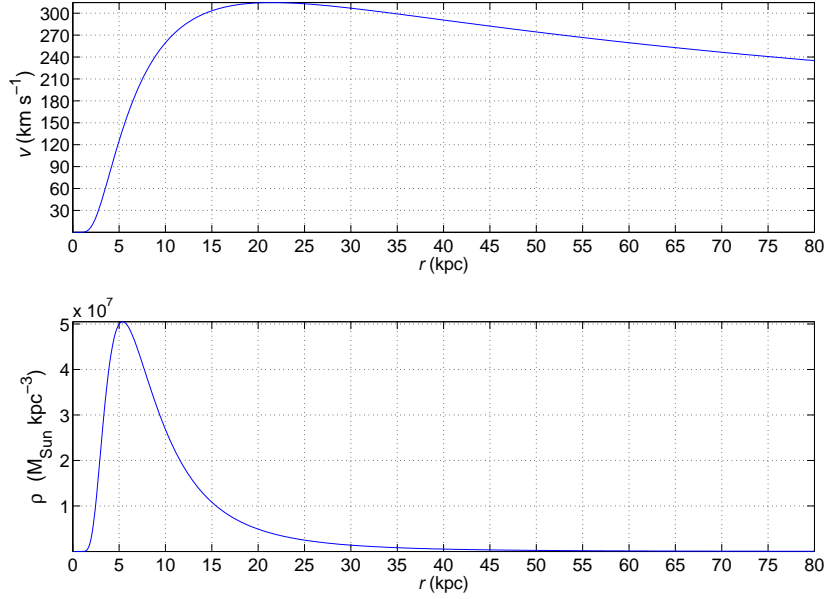


Figure 1: Upper panel: velocity rotation curve according to eq. (5). Lower panel: DM mass density profile according to eq. (2). The values $L = 21.5$ kpc and $\rho_0 = 1.077 \times 10^7 M_\odot \text{ kpc}^{-3}$ have been used.

mass effectively felt given by eq. (4); the result is

$$v_{\text{NK}} = \Omega r = 2\sqrt{\frac{\pi G \rho_0 L^3}{r}} \exp\left(-\frac{L}{2r}\right). \quad (5)$$

For

$$L = 21.5 \text{ kpc}, \quad \rho_0 = 1.077 \times 10^7 M_\odot \text{ kpc}^{-3}, \quad (6)$$

eq. (5) is able to reconstruct the observed rotation velocity curve of the Galaxy; indeed, eq. (5) yields just the observed values [9]

$$v(r_\odot) = 220 \text{ km s}^{-1}, \quad v_\infty = 235 \text{ km s}^{-1}, \quad (7)$$

where $r_\odot = 8$ kpc is the approximate distance of the Sun from the center of the Milky Way.

Oppositely, it was postulated that the Newtonian laws of gravitation have to be modified on certain acceleration scales to correctly account for

the observed anomalous kinematics of such astrophysical systems without resorting to still undetected exotic forms of matter. One of the most phenomenologically successful modification of the inverse-square Newtonian law, mainly with respect to spiral galaxies, is the MODified Newtonian Dynamics (MOND) [10, 11, 12] which postulates that for systems experiencing total gravitational acceleration $A < A_0$, with [13]

$$A_0 = 1.2 \times 10^{-10} \text{ m s}^{-2}, \quad (8)$$

$$\mathbf{A} \rightarrow \mathbf{A}_{\text{MOND}} = -\frac{\sqrt{A_0 GM}}{r} \hat{\mathbf{r}}. \quad (9)$$

More precisely, it holds

$$A = \frac{A_{\text{Newton}}}{\mu(X)}, \quad X \equiv \frac{A}{A_0}; \quad (10)$$

$\mu(X) \rightarrow 1$ for $x \gg 1$, i.e. for large accelerations (with respect to A_0), while $\mu(X) \rightarrow x$ yielding eq. (9) for $x \ll 1$, i.e. for small accelerations. The most widely used forms for μ are

$$\mu(X) = \frac{X}{1+X}, \quad [9] \quad (11)$$

$$\mu(X) = \frac{X}{\sqrt{1+X^2}} \quad [14]. \quad (12)$$

Eq. (10) strictly holds for co-planar, spherically and axially symmetric mass distributions; otherwise, the full modified (non-relativistic) Poisson equation [14]

$$\nabla \cdot \left[\mu \left(\frac{|\nabla U|}{A_0} \right) \nabla U \right] = 4\pi G\rho \quad (13)$$

must be used.

Attempts to yield a physical foundation to MOND, especially in terms of a relativistic covariant theory, can be found in, e.g., [15, 16, 17]; for recent reviews of various aspects of the MOND paradigm, see [18, 19, 20]. The compatibility of MOND with Solar System data has been investigated in [21, 22, 23, 24]. Generally speaking, many theoretical frameworks have been set up to yield a $1/r$ acceleration term able to explain the observed dynamics of astrophysical systems; for example, those encompassing a logarithmic extra-potential [25, 26]

$$U = C \ln \left(\frac{r}{r_s} \right), \quad (14)$$

where C and r_s , a length scale, are fit-for parameters. For other modified models of gravity used to explain, among other things, the galactic rotation curves without resorting to DM see, e.g., [27, 28, 29].

In this paper we wish to propose a different strategy to put MOND directly on the test in galactic scenarios; see also [30] for another approach on galactic scales, based on the escape speed in the solar neighbourhood. More specifically, we will numerically investigate the orbital dynamics of a test particle affected, in the deep-MONDian regime, by the field generated by a locally concentrated mass M to preliminarily see, at least qualitatively, if the obtained results are compatible with the observed pattern of the electromagnetically detected matter in galaxies. We will extend our analysis also to the MODified Gravity (MOG) scheme by Moffat [29] and to the action of DM itself, in the form presented above, to see if our approach is able, at least in principle, to discriminate between them. We will choose the outer ($r > 20$ kpc) regions of the Galaxy in order to avoid complications with the details of the realistic distribution of baryonic and DM matter. It is hoped that our results will encourage more quantitative and detailed studies on MOND applied to such systems; for numerical investigations on the problem of the formation of cosmological structures and galactic evolution, see [31, 32, 33, 34, 35].

2 MOND and dark matter-induced orbital motions

2.1 MOND co-planar orbital trajectories

For the sake of concreteness, we will consider a central body having about the same mass of, say, the total baryonic component of the Milky Way, i.e. [36] $M \approx 6.5 \times 10^{10} M_\odot$, and a test particle distant several tens kpc from it, acted upon by the putative MOND-like modified gravitational field of M . Let us, first, assume a total radial acceleration

$$\mathbf{A} \approx -\frac{\sqrt{A_0 G M}}{r} \hat{\mathbf{r}}, \quad (15)$$

with

$$A_0 = 1.2 \times 10^{-10} \text{ m s}^{-2} = 3,872.92 \text{ kpc Gyr}^{-2}. \quad (16)$$

In Figure 2 we plot X vs galactocentric distance according to DM, MOND and Newtonian dynamics without DM.

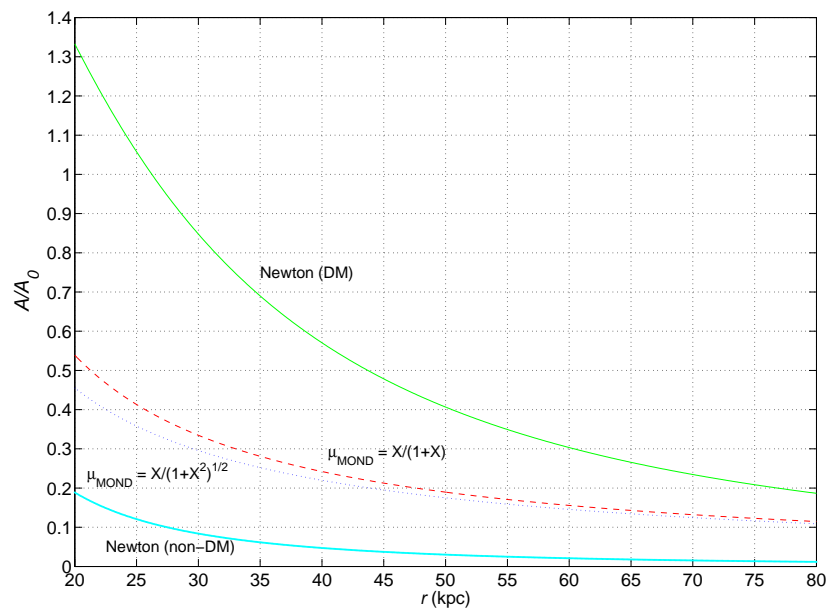


Figure 2: Ratio X of the total gravitational acceleration A , according to different models, to $A_0 = 1.2 \times 10^{-10} \text{ m s}^{-2}$ as a function of the galactocentric distance. After about 25 kpc, $X < 1$ for both DM and MOND.

Such a scenario allows to safely neglects the details of the real mass distribution which would be relevant at closer distances [37, 38] and is well suited for, e.g., a star moving in the farthest ($r \gg 10$ kpc) regions of the Galaxy by assuming the non-existence of the DM halo. Moreover, the external acceleration felt by the Milky Way in its free fall is of the order of $0.01A_0$ [39], so that certain complications that may occur in other astrophysical systems like, e.g., clusters of galaxies, [40] can be discarded. For an application of MOND to the velocity rotation curves of the Galaxy, see [9]. We will numerically integrate the equations of motion in cartesian coordinates for two non-interacting test particles at different distances from M (25 kpc and 35 kpc, respectively). In order to make realistic analysis, we used the measured, non-Keplerian velocities, reproduced by eq. (5) and Figure 1, in setting the initial conditions corresponding to co-planar, circular orbits. The result is depicted in Figure 3; the dashed lines correspond to the Newtonian circular orbits integrated with the Keplerian initial velocities (without DM). The temporal interval spanned by the integration is of the order of Gyr, corresponding to the (Keplerian) orbital period of the farthest particle.

Until now we have used the approximated form of eq. (9) for the acceleration experienced by the test particle in the deep MOND regime; in Figure 4 and Figure 5 we show the effects of eq. (4) and eq. (5) which yield

$$A_1 = \frac{GM}{2r^2} \left(1 + \sqrt{1 + \frac{4A_0 r^2}{GM}} \right), \quad \mu = \frac{X}{1+X}, \quad (17)$$

$$A_2 = \frac{GM}{r^2} \sqrt{\frac{1}{2} + \frac{1}{2} \sqrt{1 + \left(\frac{2A_0 r^2}{GM} \right)^2}}, \quad \mu = \frac{X}{\sqrt{1+X^2}}, \quad (18)$$

respectively. The approximated MOND acceleration of eq. (9) ($\mu = X$) and eq. (18) yield quite similar results, contrary to eq. (17) whose effects are, instead, quantitatively smaller.

For even farther regions (50-70 kpc), the patterns are depicted in Figure 6 ($\mu = X$), Figure 7 ($\mu = X/(1+X)$) and Figure 8 ($\mu = X/\sqrt{1+X^2}$).

The most striking issue that our analysis raises is, perhaps, the fact that all the MOND-type accelerations considered clearly does not yield co-planar circular orbits, which contradicts one of the assumptions on which the phenomenological success of MOND (and of DM as well) is based in explaining the galactic rotational curves, i.e. the circularity of the orbits of the electromagnetically detectable baryonic matter. Second, one may wonder if the predicted MONDian orbital configurations are compatible with the real dis-

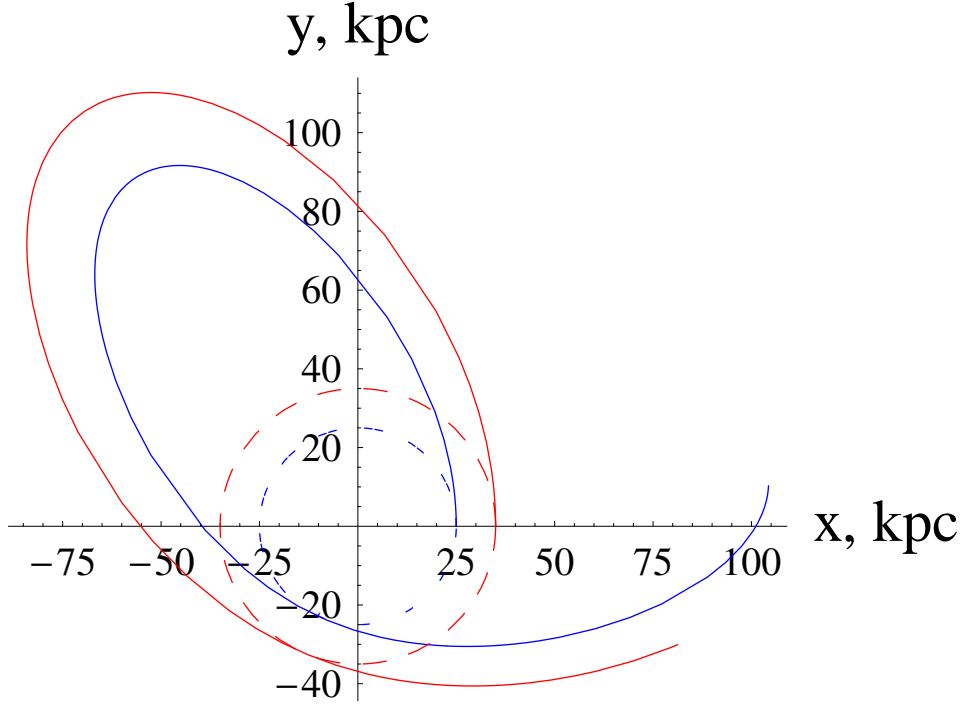


Figure 3: Numerically integrated trajectories of two test particles around a mass $M = 6.5 \times 10^{10} M_{\odot}$, located at the origin, affected by the approximated MOND acceleration $\sqrt{A_0 GM}/r$. For both particles (1) and (2) the non-Keplerian velocities ($\dot{x}_0^{(1/2)} = \dot{z}_0^{(1/2)} = 0$, $\dot{y}_0^{(1/2)} = v_{\text{NK}}^{(1/2)}$) given by eq. (5) and Figure 1 were assumed in the initial conditions corresponding to co-planar motions with $x_0^{(1)} = 25$ kpc, $y_0^{(1)} = z_0^{(1)} = 0$ (blue line), $x_0^{(2)} = 35$ kpc, $y_0^{(2)} = z_0^{(2)} = 0$ (red line). The dashed circles are the Newtonian orbits with Keplerian (without DM) initial velocities for $x_0 = a(1 - e)$, $y_0 = 0$, $z_0 = 0$, $\dot{x}_0 = 0$, $\dot{y}_0 = na\sqrt{(1 + e)/(1 - e)}$, $\dot{z}_0 = 0$ with $a_1 = 25$ kpc (blue line), $a_2 = 35$ kpc (red line), and $e_1 = e_2 = 0.0$; a and e are the Keplerian semi-major axis and eccentricity, respectively, while $n = \sqrt{GM/a^3}$ is the Keplerian mean motion. The integration spans about 2.5 Gyr corresponding to the Keplerian orbital period of the outer particle.

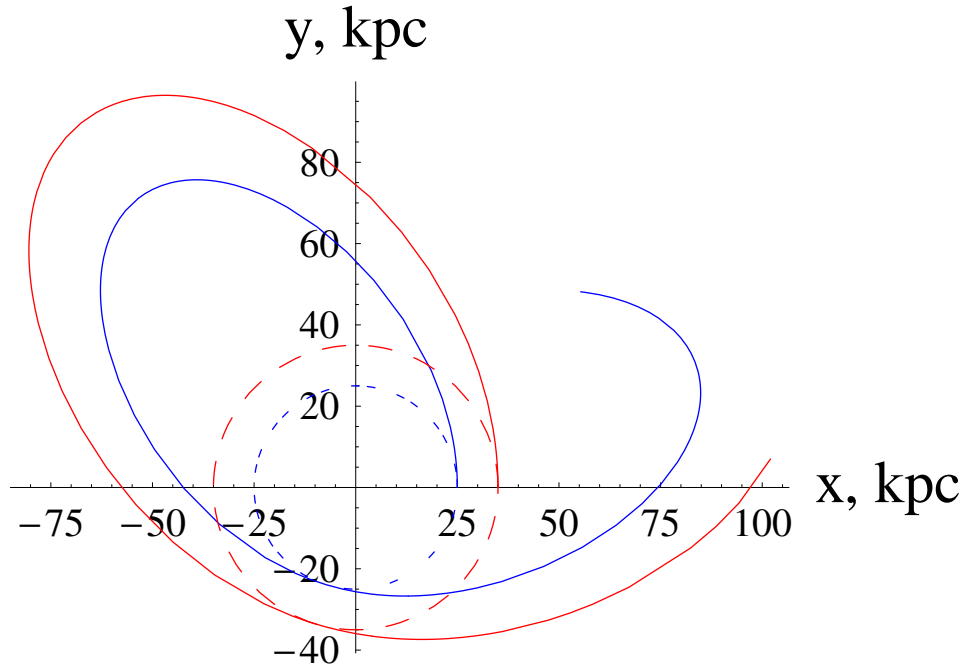


Figure 4: Numerically integrated trajectories of two test particles around a mass $M = 6.5 \times 10^{10} M_{\odot}$, located at the origin, affected by eq. (17) for $\mu = X/(1 + X)$. For both particles (1) and (2) the non-Keplerian velocities ($\dot{x}_0^{(1/2)} = \dot{z}_0^{(1/2)} = 0, \dot{y}_0^{(1/2)} = v_{\text{NK}}^{(1/2)}$) were assumed in the initial conditions corresponding to co-planar motions with $x_0^{(1)} = 25$ kpc, $y_0^{(1)} = z_0^{(1)} = 0, x_0^{(2)} = 35$ kpc, $y_0^{(2)} = z_0^{(2)} = 0$.

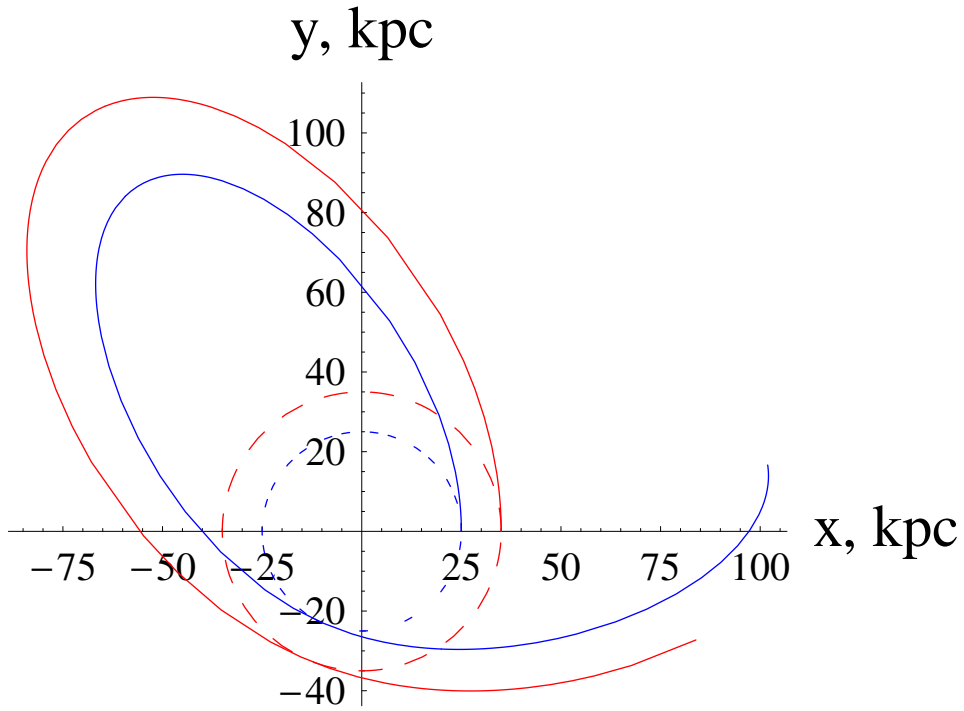


Figure 5: Numerically integrated trajectories of two test particles around a mass $M = 6.5 \times 10^{10} M_{\odot}$, located at the origin, affected by eq. (18) for $\mu = X/\sqrt{1+X^2}$. For both particles (1) and (2) the non-Keplerian velocities ($\dot{x}_0^{(1/2)} = \dot{z}_0^{(1/2)} = 0, \dot{y}_0^{(1/2)} = v_{\text{NK}}^{(1/2)}$) were assumed in the initial conditions corresponding to co-planar motions with $x_0^{(1)} = 25$ kpc, $y_0^{(1)} = z_0^{(1)} = 0, x_0^{(2)} = 35$ kpc, $y_0^{(2)} = z_0^{(2)} = 0$.

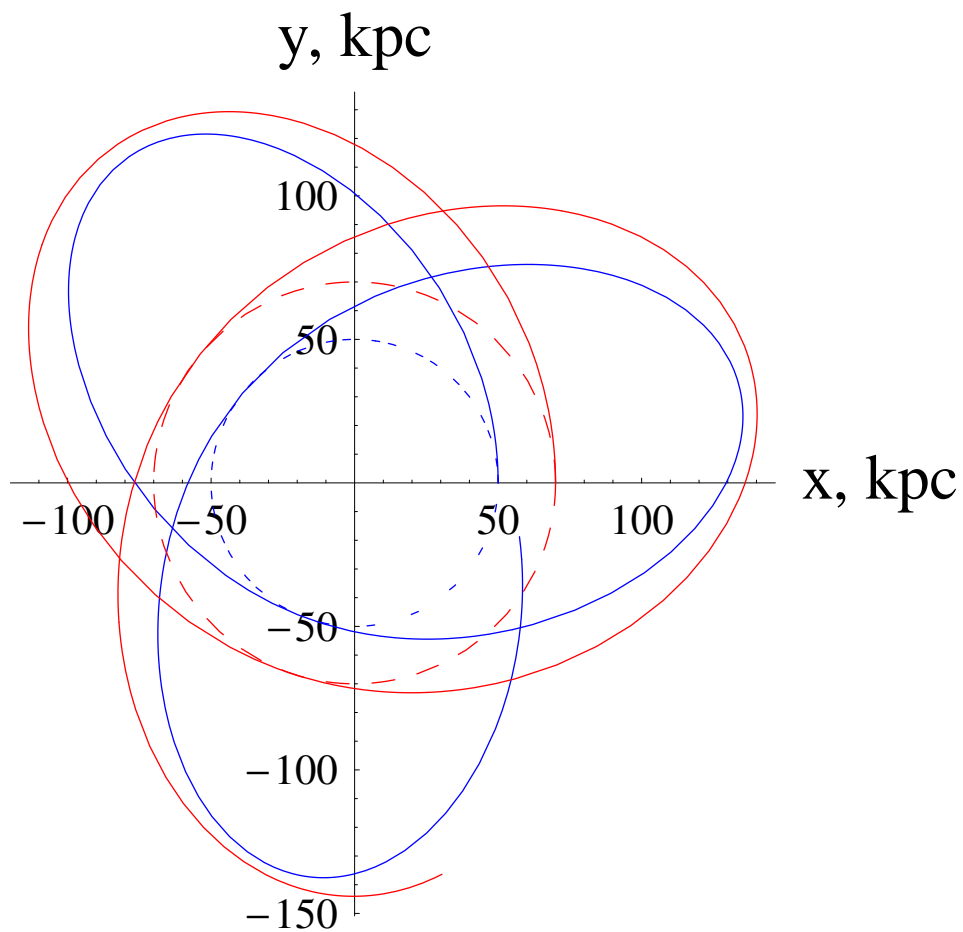


Figure 6: Numerically integrated trajectories of two test particles around a mass $M = 6.5 \times 10^{10} M_{\odot}$, located at the origin, affected by the approximated MOND acceleration $\sqrt{A_0 GM}/r$ ($\mu = X$). For both particles (1) and (2) the non-Keplerian velocities ($\dot{x}_0^{(1/2)} = \dot{z}_0^{(1/2)} = 0, y_0^{(1/2)} = v_{\text{NK}}^{(1/2)}$) were assumed in the initial conditions corresponding to coplanar motions with $x_0^{(1)} = 50$ kpc, $y_0^{(1)} = z_0^{(1)} = 0$ (blue line), $x_0^{(2)} = 70$ kpc, $y_0^{(2)} = z_0^{(2)} = 0$ (red line). The Newtonian orbits (dashed lines) have been integrated with the Keplerian (without DM) initial velocities. The Newtonian accelerations amount to about 1% of A_0 .

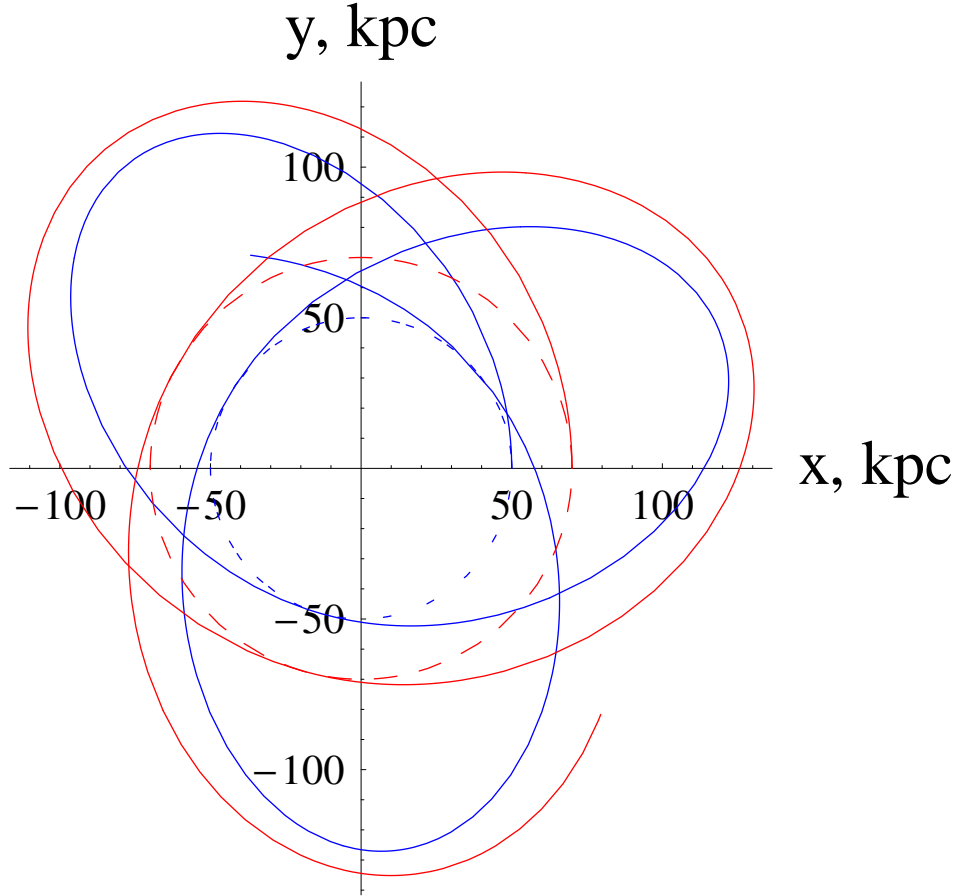


Figure 7: Numerically integrated trajectories of two test particles around a mass $M = 6.5 \times 10^{10} M_{\odot}$, located at the origin, affected by the MOND acceleration of eq. (17) ($\mu = X/(1 + X)$). For both particles (1) and (2) the non-Keplerian velocities ($\dot{x}_0^{(1/2)} = \dot{z}_0^{(1/2)} = 0, y_0^{(1/2)} = v_{\text{NK}}^{(1/2)}$) were assumed in the initial conditions corresponding to coplanar motions with $x_0^{(1)} = 50$ kpc, $y_0^{(1)} = z_0^{(1)} = 0$, $x_0^{(2)} = 70$ kpc, $y_0^{(2)} = z_0^{(2)} = 0$. The Newtonian orbits (dashed lines) have been integrated with the Keplerian (without DM) initial velocities.

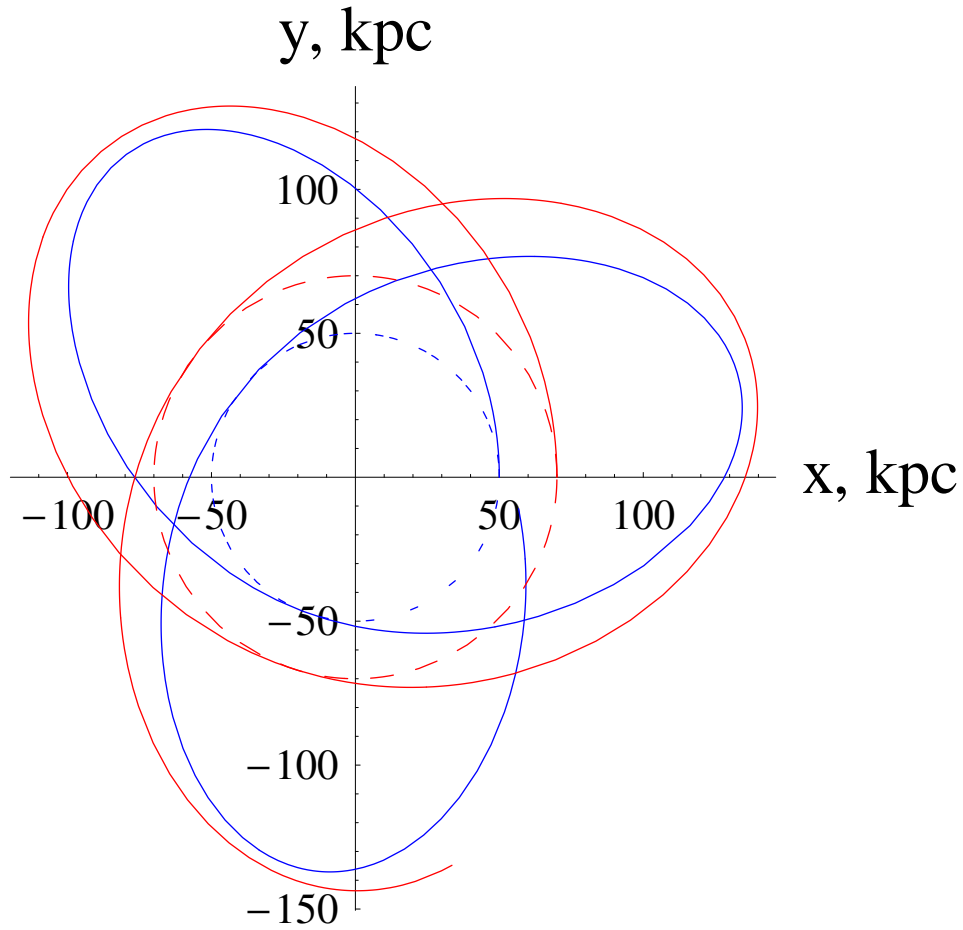


Figure 8: Numerically integrated trajectories of two test particles around a mass $M = 6.5 \times 10^{10} M_{\odot}$, located at the origin, affected by the MOND acceleration of eq. (18) ($\mu = X/\sqrt{1+X^2}$). For both particles (1) and (2) the non-Keplerian velocities ($\dot{x}_0^{(1/2)} = \dot{z}_0^{(1/2)} = 0, \dot{y}_0^{(1/2)} = v_{\text{NK}}^{(1/2)}$) were assumed in the initial conditions corresponding to coplanar motions with $x_0^{(1)} = 50$ kpc, $y_0^{(1)} = z_0^{(1)} = 0$, $x_0^{(2)} = 70$ kpc, $y_0^{(2)} = z_0^{(2)} = 0$. The Newtonian orbits (dashed lines) have been integrated with the Keplerian (without DM) initial velocities.

tribution of the electromagnetically-detectable baryonic matter (stars+gas) in such remote regions of the galaxies in the sense that if, for $r \gtrsim 10$ kpc, there was enough ordinary matter, it should statistically fill the orbital patterns shown. It is certainly difficult to have, at present, observations which are both accurate enough and sufficiently abundant in such remote regions of the galaxies, but our analysis may drive further observational surveys towards the implementation of this goal.

2.2 DM co-planar orbital trajectories

What is the influence of DM, modelled as in Section 1, on the orbital motion of test particles moving in the outer regions of a galaxy? We will integrate the equations of motion with the acceleration of eq. (4) and the values of eq. (6) corresponding to the Galaxy; the initial conditions are the same as the MOND case of Figure 3; in particular, we used the measured velocities, reproduced by eq. (5) and Figure 1, in setting the initial conditions; also in this case, the dashed lines represent the orbits integrated by using the Keplerian (without DM) velocities. The result is in Figure 9. The orbital pattern looks radically different with respect to the MONDian one of Figure 3. Notable differences also occur in the farthest (50 – 70 kpc) regions, as shown by Figure 10. Indeed, contrary to MOND, the effective DM density of eq. (2) yields circular, co-planar orbits also in the remote periphery of galaxies; this would allow, in principle, for the possibility of discriminating between MOND and DM.

A similar analysis, although for distances below 20 kpc, has been recently performed in Ref. [37]. Its authors analyze the non-planar motion of the Sagittarius dwarf galaxy, orbiting at 17 kpc from the Milky Way center, by comparing DM haloes characterized by different spatial symmetries to MOND with a more detailed model of mass distribution finding very close similarities in the resulting orbital motions. The out-of-plane dynamics at close ($r \ll 20$ kpc) Galactocentric distances as a possible way to distinguish MOND from DM has been investigated also in Ref. [38], but it was found difficult to practically implement in realistic scenarios with current observations. In Section 2.3 we will deal with the out-of-plane motions.

2.3 Non-planar orbits: MOND and DM

MOND and DM yields different non-planar orbits as well. This can be shown in deep MOND regime by considering the Small Magellanic Cloud (SMC) located at 59 kpc from the center of the Milky Way; SMC's galactocentric

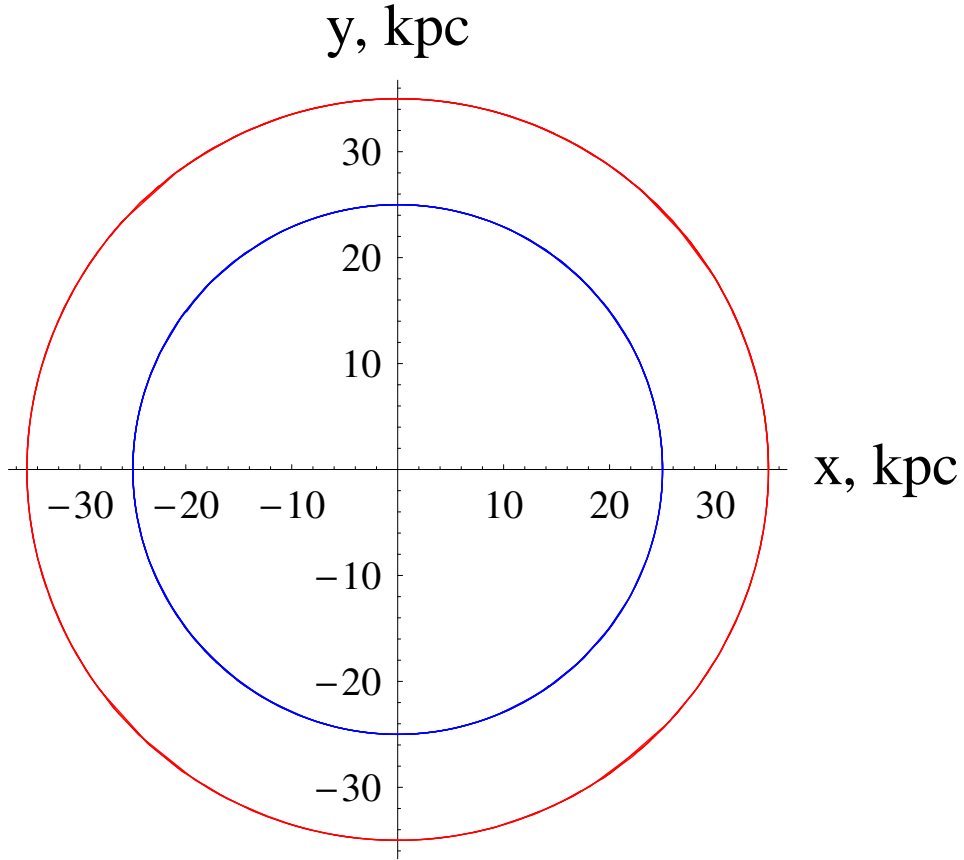


Figure 9: Numerically integrated trajectories of two test particles acted upon by the DM acceleration of eq. (4) with $L = 21.5$ kpc and $\rho_0 = 1.077 \times 10^7 M_\odot \text{ kpc}^{-3}$. The same initial conditions of the MOND case of Figure 3-Figure 5 were adopted. In particular, non-Keplerian initial velocities (eq. (5) and Figure 1) for the DM-induced orbits and Keplerian velocities (without DM) for the Newtonian trajectories were used.

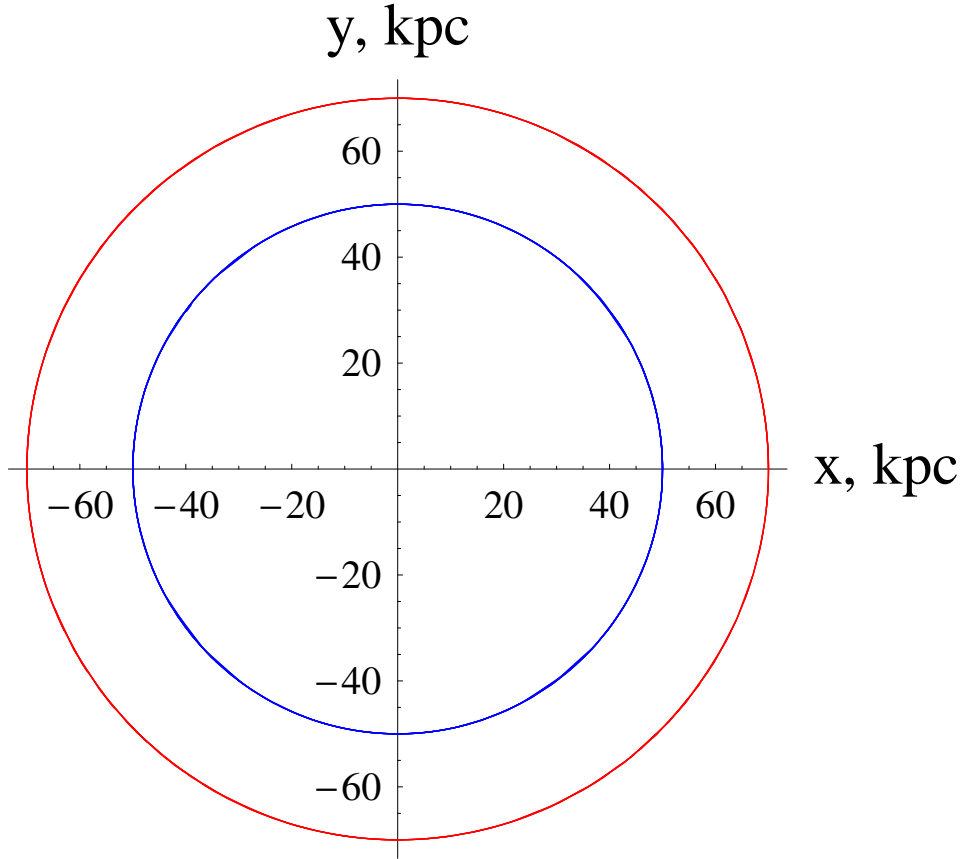


Figure 10: Numerically integrated trajectories of two test particles acted upon by the DM acceleration of eq. (4) with $L = 21.5$ kpc and $\rho_0 = 1.077 \times 10^7 M_\odot \text{ kpc}^{-3}$. For both particles (1) and (2) the non-Keplerian velocities ($\dot{x}_0^{(1/2)} = \dot{z}_0^{(1/2)} = 0, \dot{y}_0^{(1/2)} = v_{\text{NK}}^{(1/2)}$) were assumed in the initial conditions corresponding to co-planar motions with $x_0^{(1)} = 50$ kpc, $y_0^{(1)} = z_0^{(1)} = 0, x_0^{(2)} = 70$ kpc, $y_0^{(2)} = z_0^{(2)} = 0$. The Newtonian orbits (dashed lines) were integrated with the Keplerian (without DM) initial velocities.

Table 1: Galactocentric coordinates (in kpc) and velocity components (in km s^{-1}) of SMC [41]. They yield $r = 58.9$ kpc, $v = 302 \pm 52$ km s^{-1} .

$x_0 = 15.3$ kpc	$y_0 = -36.9$ kpc	$z_0 = -43.3$ kpc
$\dot{x}_0 = -87 \pm 48$ km s^{-1}	$\dot{y}_0 = -247 \pm 42$ km s^{-1}	$\dot{z}_0 = 149 \pm 37$ km s^{-1}

coordinates and velocities [41] are quoted in Table 1.

Figure 1 and eq. (5) yield $v = 261$ km s^{-1} for $r = 59$ kpc, which is compatible with the SMC measured velocity of Table 1; thus, we can safely use our effective DM model to integrate the equations of motion of SMC. The results for an integration over 10 Gyr backward in time are in Figure 11 - Figure 14

MOND yields quite different results, as depicted in Figure 15- Figure 18 in which we used $\mu = X/\sqrt{1+X^2}$; $\mu = X$ and $\mu = X/(1+X)$ yield substantially similar plots, so that we decided not to insert them. Apart from the evident qualitative differences between DM and MOND, also from the quantitative point of view MOND is different from DM since it allows for wider excursions, up to 200 kpc in the y direction, contrary to 100 kpc of DM.

3 MOG orbital trajectories

Let us, now, repeat the same calculations as before with the MOdified Grav-ity (MOG) model [29]. It is a fully covariant theory of gravity which is based on the existence of a massive vector field coupled universally to matter. The theory yields a Yukawa-like modification of gravity with three constants which, in the most general case, are running; they are present in the theory's action as scalar fields which represent the gravitational constant, the vector field coupling constant, and the vector field mass. An approximate solution of the MOG field equations [42] allows to compute their values as functions of the source's mass.

The resulting Yukawa-type modification of the inverse-square Newton's law in the gravitational field of a central mass M is

$$\mathbf{A}_{\text{MOG}} = -\frac{G_{\text{N}}M}{r^2} \{1 + \alpha [1 - (1 + \mu r) \exp(-\mu r)]\} \hat{\mathbf{r}}, \quad (19)$$

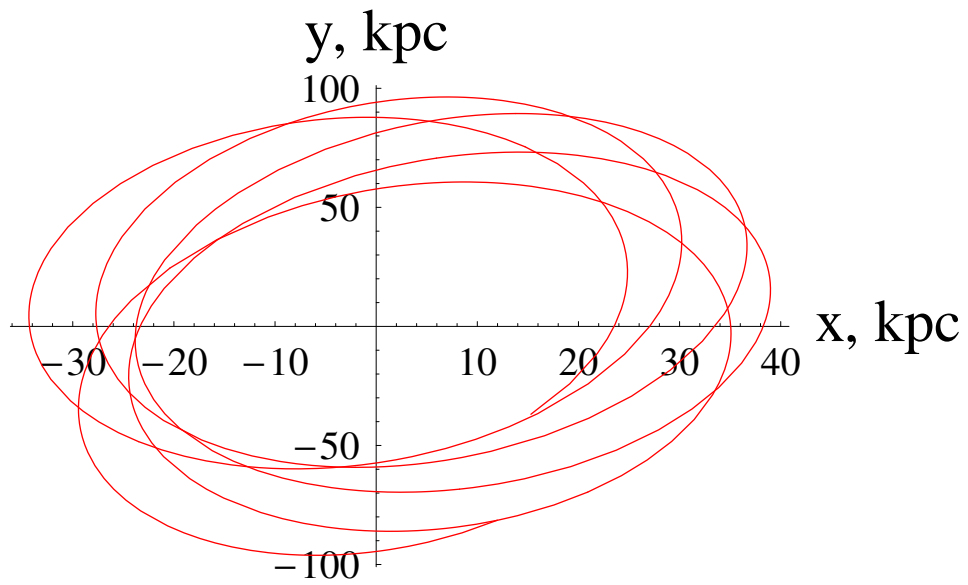


Figure 11: Section in the $\{xy\}$ plane of the numerically integrated trajectory of SMC experiencing the DM acceleration of eq. (4) with $L = 21.5$ kpc and $\rho_0 = 1.077 \times 10^7 M_\odot \text{kpc}^{-3}$ for the central values of the initial conditions of Table 1. The time span of the integration is 10 Gyr backward in time.

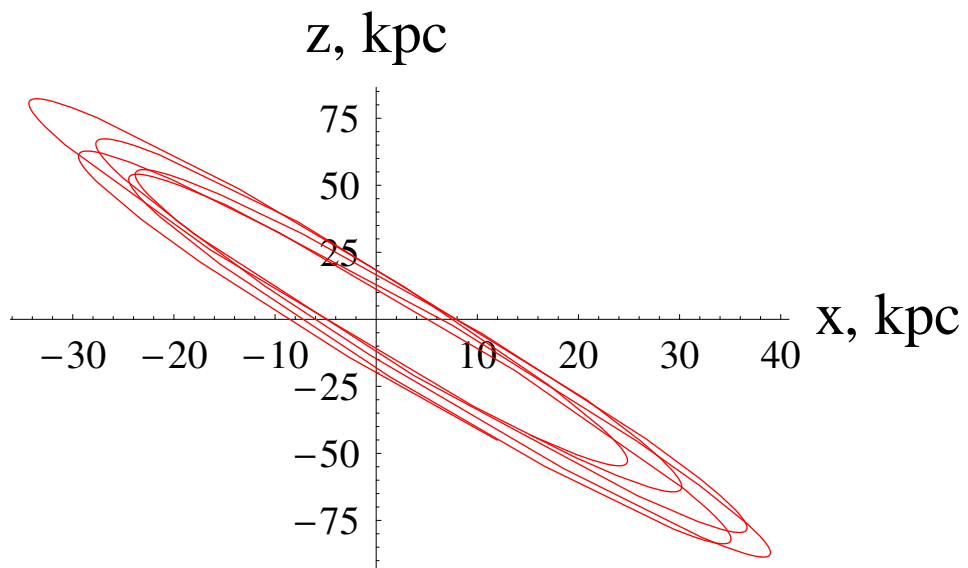


Figure 12: Section in the $\{xz\}$ plane of the numerically integrated trajectory of SMC experiencing the DM acceleration of eq. (4) with $L = 21.5$ kpc and $\rho_0 = 1.077 \times 10^7 M_\odot \text{kpc}^{-3}$ for the central values of the initial conditions of Table 1. The time span of the integration is 10 Gyr backward in time.

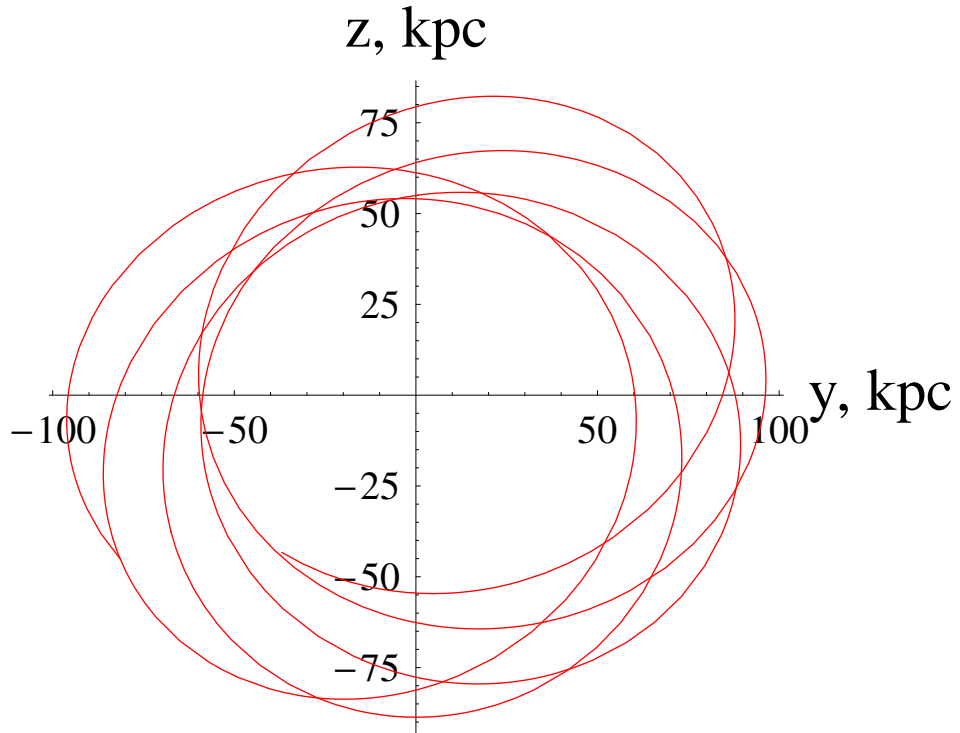
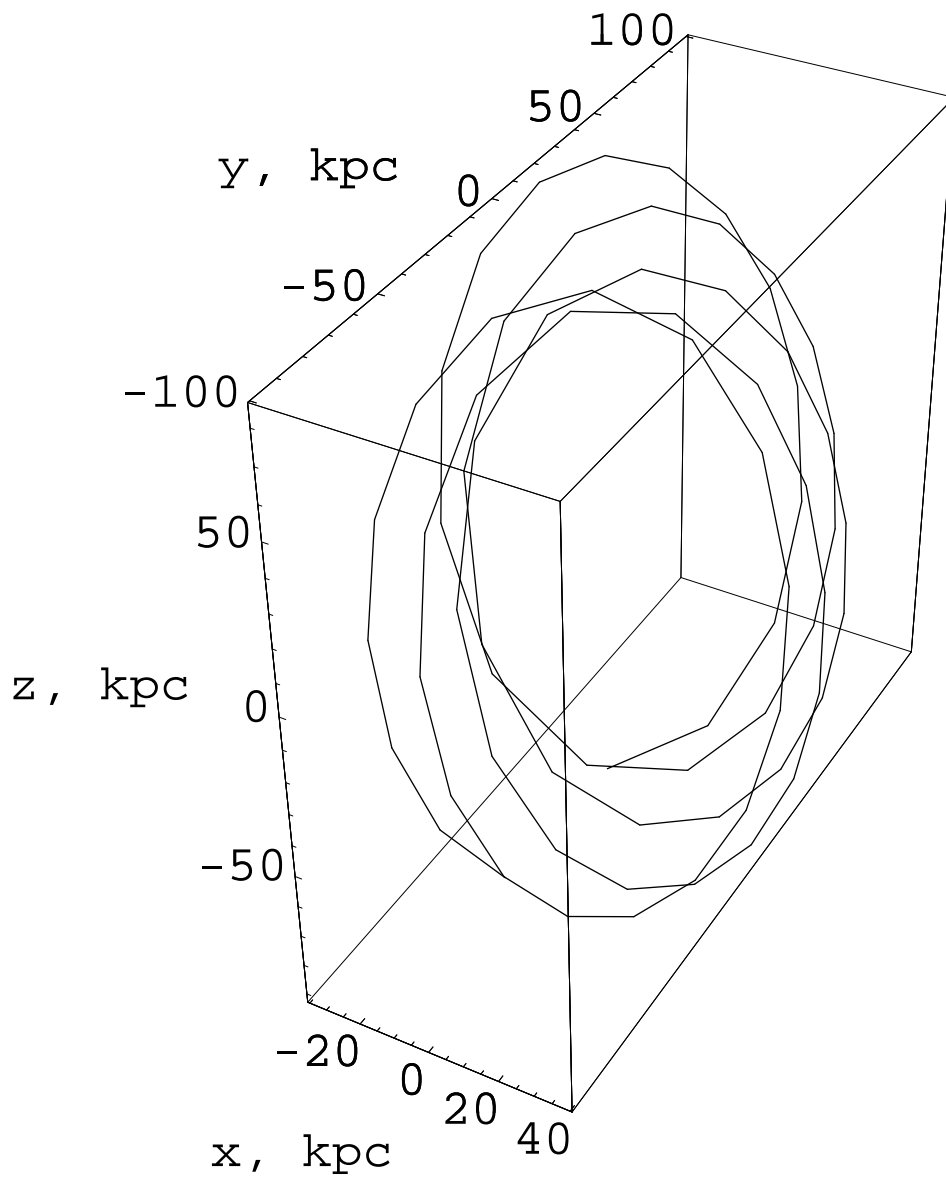


Figure 13: Section in the $\{yz\}$ plane of the numerically integrated trajectory of SMC experiencing the DM acceleration of eq. (4) with $L = 21.5$ kpc and $\rho_0 = 1.077 \times 10^7 M_\odot \text{ kpc}^{-3}$ for the central values of the initial conditions of Table 1. The time span of the integration is 10 Gyr backward in time.



21
 Figure 14: Numerically integrated trajectory of SMC experiencing the DM acceleration of eq. (4) with $L = 21.5$ kpc and $\rho_0 = 1.077 \times 10^7 M_\odot \text{ kpc}^{-3}$ for the central values of the initial conditions of Table 1. The integration time span is 10 Gyr backward in time.

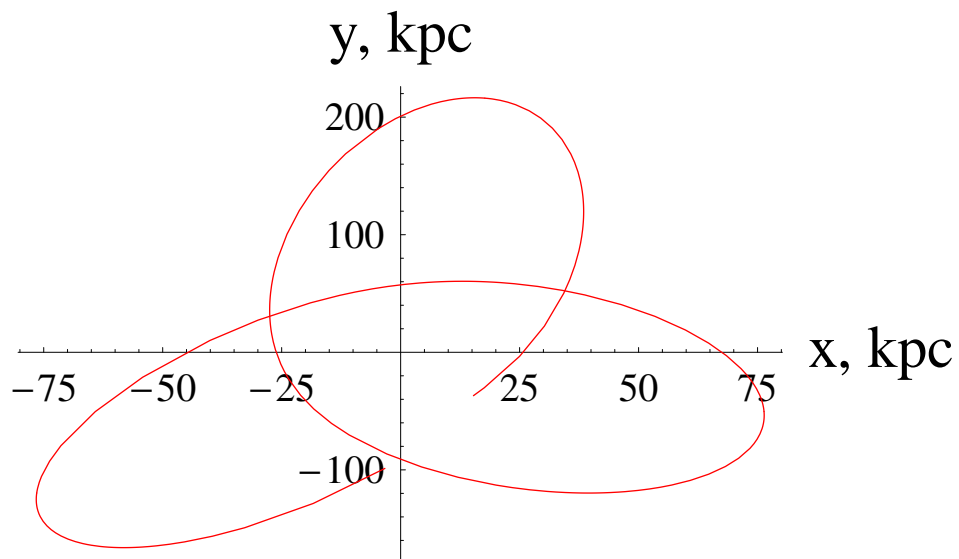


Figure 15: Section in the $\{xy\}$ plane of the numerically integrated trajectory of SMC around a mass $M = 6.5 \times 10^{10} M_{\odot}$, located at the origin, affected by the MOND acceleration of eq. (18) ($\mu = X/\sqrt{1+X^2}$) for the central values of the initial conditions of Table 1. The time span of the integration is 10 Gyr backward in time.

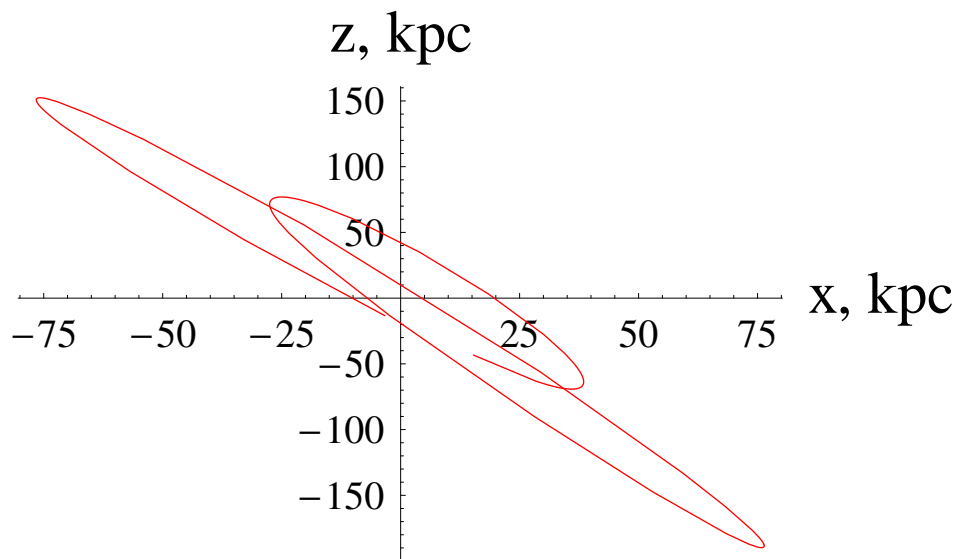


Figure 16: Section in the $\{xz\}$ plane of the numerically integrated trajectory of SMC around a mass $M = 6.5 \times 10^{10} M_{\odot}$, located at the origin, affected by the MOND acceleration of eq. (18) ($\mu = X/\sqrt{1+X^2}$) for the central values of the initial conditions of Table 1. The time span of the integration is 10 Gyr backward in time.

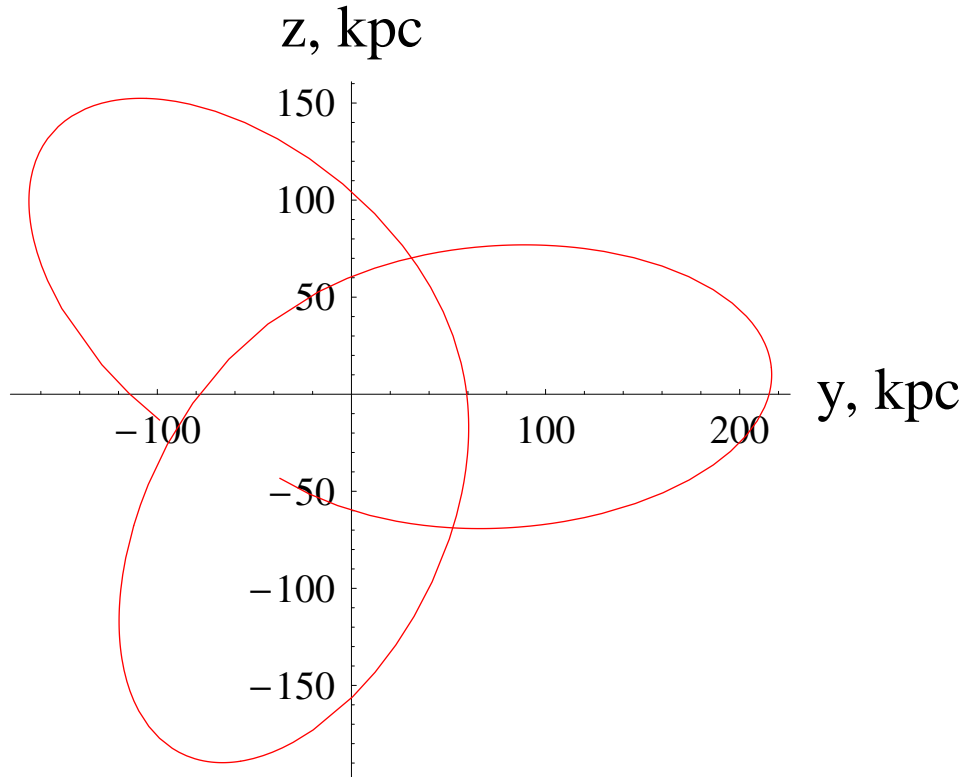


Figure 17: Section in the $\{yz\}$ plane of the numerically integrated trajectory of SMC around a mass $M = 6.5 \times 10^{10} M_{\odot}$, located at the origin, affected by the MOND acceleration of eq. (18) ($\mu = X/\sqrt{1+X^2}$) for the central values of the initial conditions of Table 1. The time span of the integration is 10 Gyr backward in time.

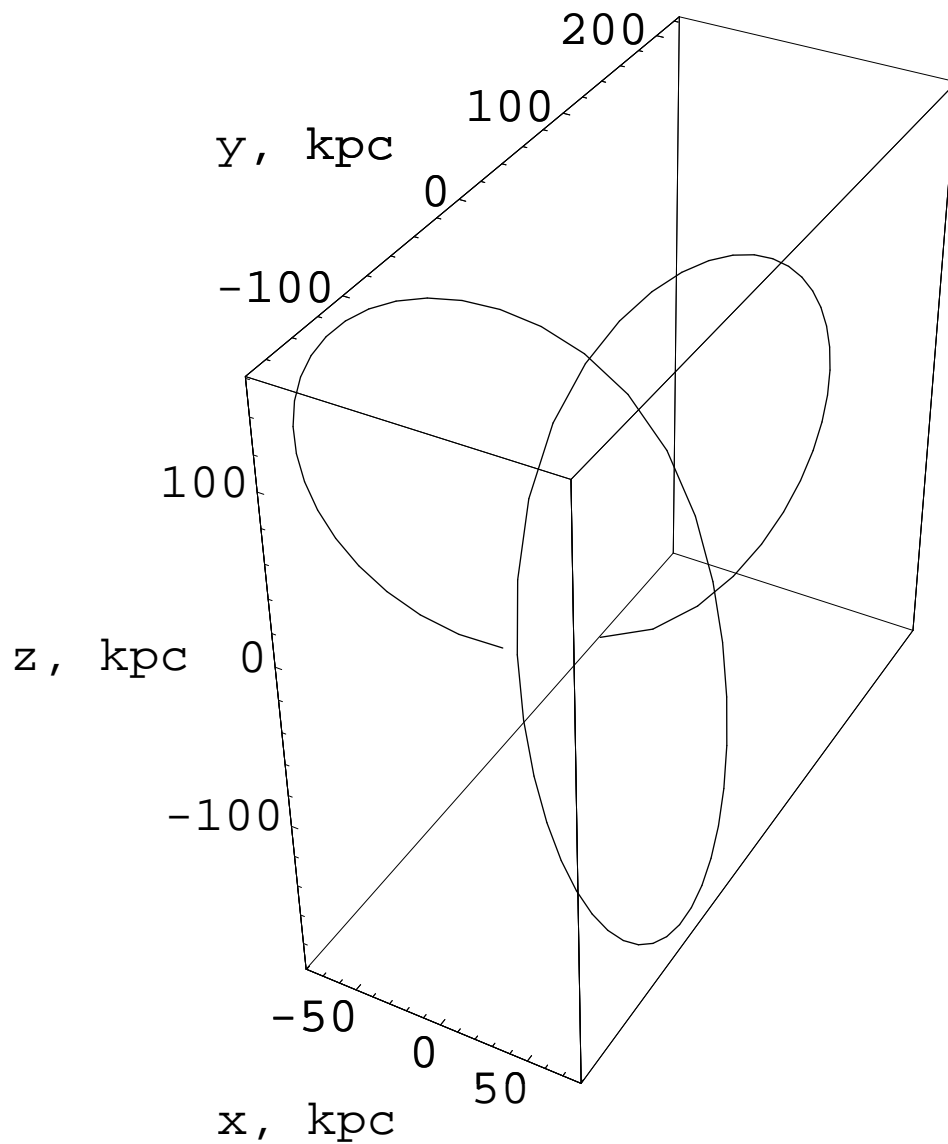


Figure 18: Numerically integrated trajectories of SMC around a mass $M = 6.5 \times 10^{10} M_{\odot}$, located at the origin, affected by the MOND acceleration of eq. (18) ($\mu = X/\sqrt{1+X^2}$) for the central values of the initial conditions of Table 1. The integration time span is 10 Gyr backward in time.

with

$$\alpha \simeq \frac{M}{\left(\sqrt{M} + C'_1\right)^2} \left(\frac{G_\infty}{G_N} - 1\right), \quad (20)$$

$$\mu \simeq \frac{C'_2}{\sqrt{M}}, \quad (21)$$

where G_N is the Newtonian gravitational constant and

$$G_\infty \simeq 20G_N, \quad (22)$$

$$C'_1 \simeq 25,000\sqrt{M_\odot}, \quad (23)$$

$$C'_2 \simeq 6,250\sqrt{M_\odot} \text{ kpc}^{-1}. \quad (24)$$

Such values have been obtained in [42] as a result of the fit of the velocity rotation curves of some galaxies in the framework of the searches for an explanation of the rotation curves of galaxies without resorting to DM.

The validity of eq. (19) in the Solar System has been recently questioned in [43].

For $M = 6.5 \times 10^{10} M_\odot$ we have

$$\alpha \simeq 16 \quad (25)$$

$$\lambda = \frac{1}{\mu} \simeq 41 \text{ kpc}. \quad (26)$$

In Figure 19 we show the outcome of the numerical integration of eq. (19) for two test particles at 25 kpc and 35 kpc from M ; also in this case, we used the observed non-Keplerian velocities (eq. (5), Figure 1) for the initial conditions, while the Keplerian ones (without DM) were adopted for the integration of the Newtonian orbits. The resulting orbital patterns looks like the the MONDian ones (Figure 3-Figure 5) and are in contrast with those produced by DM.

The situation for the 50-70 kpc region is depicted in Figure 20; cfr. with Figure 6-Figure 8.

The action of MOG on non-planar orbits is depicted in Figure 24 in the case of SMC with the same initial conditions of Section 2.3.

In this case, the orbital patterns present not only differences with respect to DM, but also to MOND, although at lesser extent.

4 Summary and conclusions

In this paper we investigated the orbital dynamics of test particles in the remote ($r \approx 25 - 70$ kpc) periphery of a typical spiral galaxy both in the

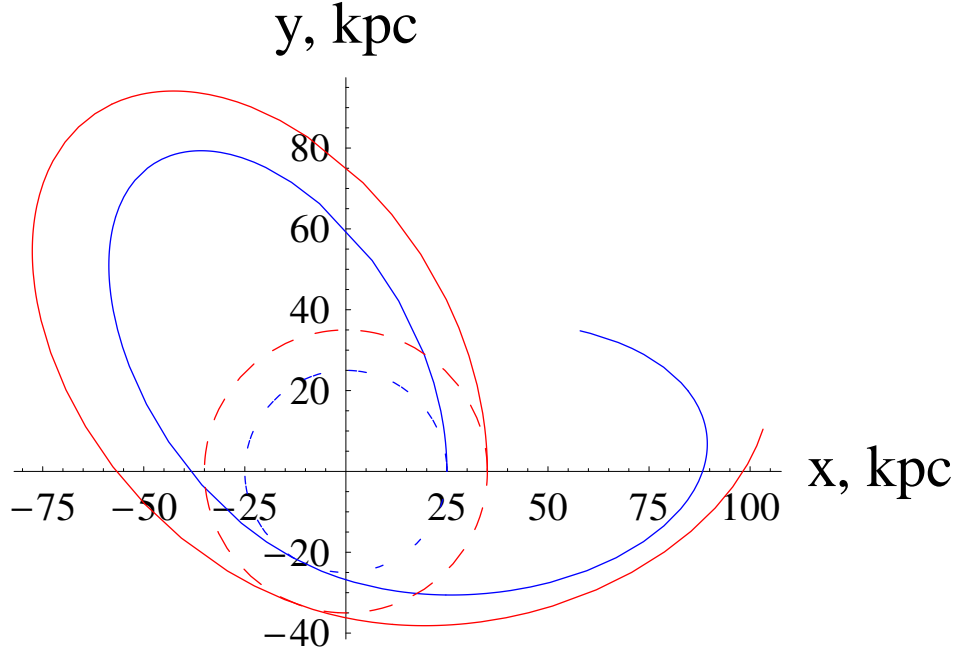


Figure 19: Numerically integrated trajectories of two test particles around a mass $M = 6.5 \times 10^{10} M_{\odot}$, located at the origin, affected by the MOG acceleration of eq. (19). For both particles (1) and (2) the non-Keplerian velocities ($\dot{x}_0^{(1/2)} = \dot{z}_0^{(1/2)} = 0, \dot{y}_0^{(1/2)} = v_{\text{NK}}^{(1/2)}$) given by eq. (5) and Figure 1 were assumed in the initial conditions corresponding to coplanar motions with $x_0^{(1)} = 25$ kpc, $y_0^{(1)} = z_0^{(1)} = 0$, $x_0^{(2)} = 35$ kpc, $y_0^{(2)} = z_0^{(2)} = 0$. The dashed circles are the Newtonian orbits with Keplerian (without DM) initial velocities for $x_0 = a(1 - e)$, $y_0 = 0$, $z_0 = 0$, $\dot{x}_0 = 0$, $\dot{y}_0 = na\sqrt{(1 + e)/(1 - e)}$, $\dot{z}_0 = 0$ with $a_1 = 25$ kpc (blue line), $a_2 = 35$ kpc (red line), and $e_1 = e_2 = 0.0$. The integration spans about 2.5 Gyr corresponding to the (Keplerian, no DM) orbital period of the outer particle. It turns out $\alpha = 16$, $1/\mu = 41$ kpc.

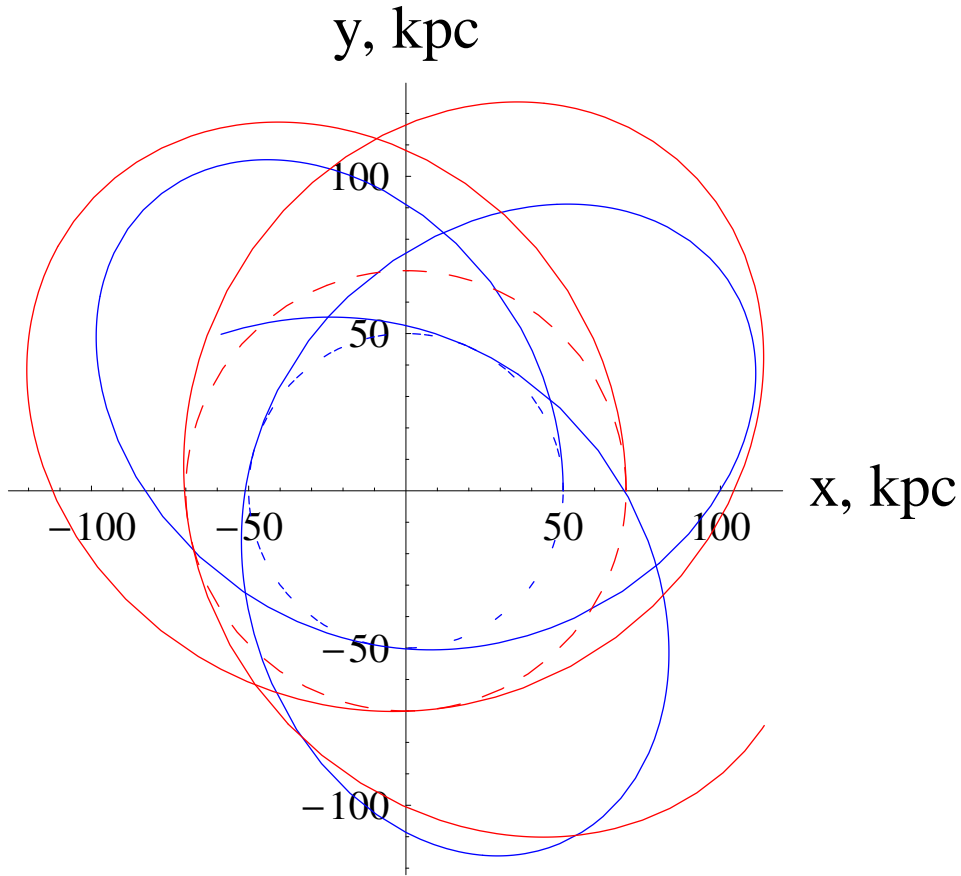


Figure 20: Numerically integrated trajectories of two test particles around a mass $M = 6.5 \times 10^{10} M_{\odot}$, located at the origin, affected by the MOG acceleration of eq. (19). For both particles (1) and (2) the non-Keplerian velocities ($\dot{x}_0^{(1/2)} = \dot{z}_0^{(1/2)} = 0, \dot{y}_0^{(1/2)} = v_{\text{NK}}^{(1/2)}$) given by eq. (5) and Figure 1 were assumed in the initial conditions corresponding to coplanar motions with $x_0^{(1)} = 50$ kpc, $y_0^{(1)} = z_0^{(1)} = 0, x_0^{(2)} = 70$ kpc, $y_0^{(2)} = z_0^{(2)} = 0$. The dashed circles are the Newtonian orbits with Keplerian (without DM) initial velocities for $x_0 = a(1 - e), y_0 = 0, z_0 = 0, \dot{x}_0 = 0, \dot{y}_0 = na\sqrt{(1 + e)/(1 - e)}, \dot{z}_0 = 0$ with $a_1 = 50$ kpc (blue line), $a_2 = 70$ kpc (red line), and $e_1 = e_2 = 0.0$.

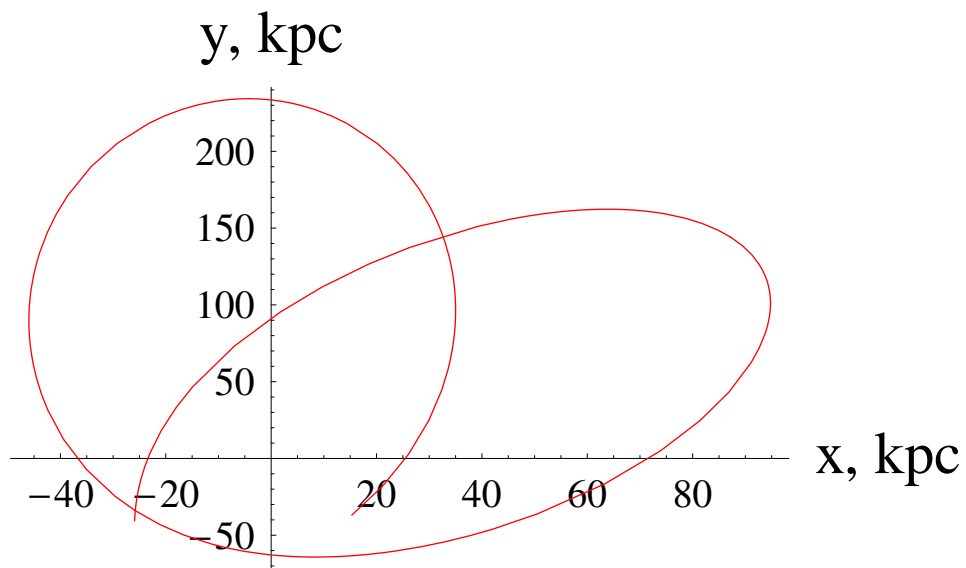


Figure 21: Section in the $\{xy\}$ plane of the numerically integrated trajectory of SMC around a mass $M = 6.5 \times 10^{10} M_{\odot}$, located at the origin, affected by the MOG acceleration of eq. (19) for the central values of the initial conditions of Table 1. The time span of the integration is 10 Gyr backward in time.

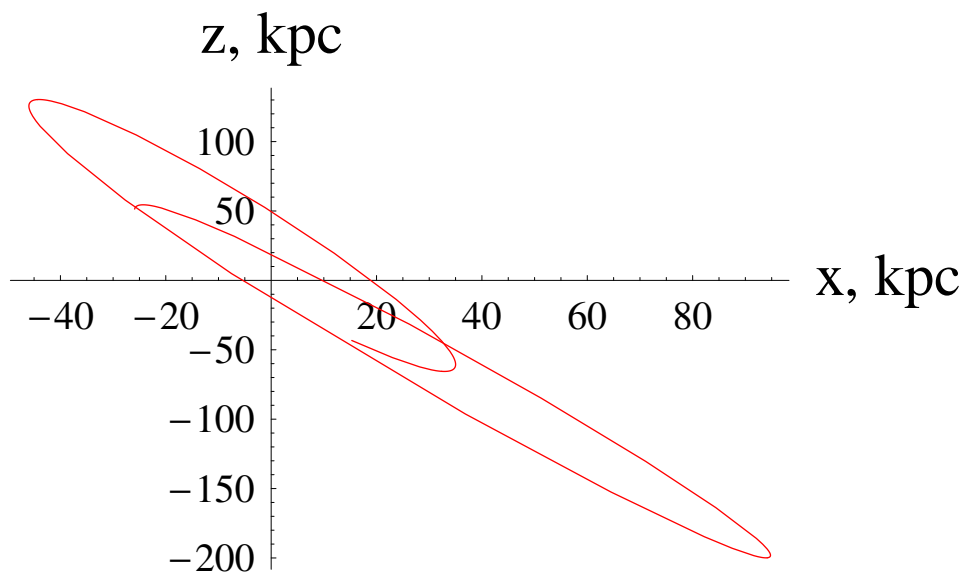


Figure 22: Section in the $\{xz\}$ plane of the numerically integrated trajectory of SMC around a mass $M = 6.5 \times 10^{10} M_{\odot}$, located at the origin, affected by the MOG acceleration of eq. (19) for the central values of the initial conditions of Table 1. The time span of the integration is 10 Gyr backward in time.

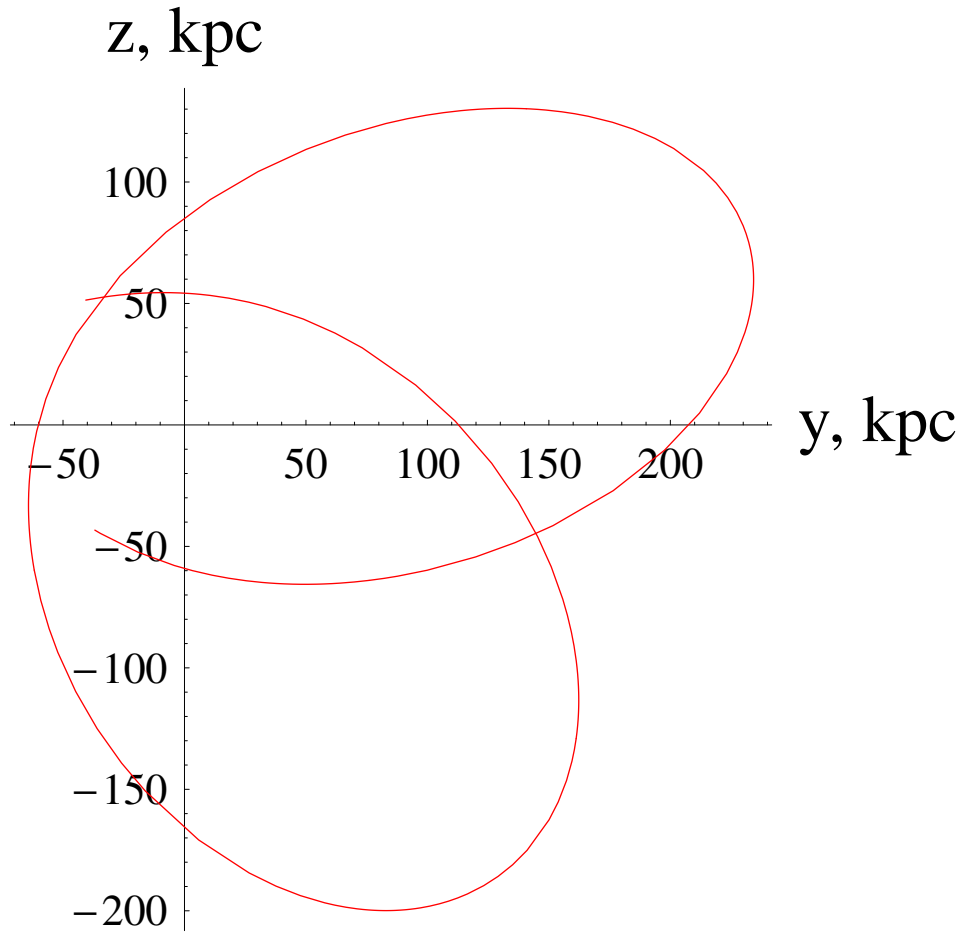


Figure 23: Section in the $\{yz\}$ plane of the numerically integrated trajectory of SMC around a mass $M = 6.5 \times 10^{10} M_{\odot}$, located at the origin, affected by the MOG acceleration of eq. (19) for the central values of the initial conditions of Table 1. The time span of the integration is 10 Gyr backward in time.

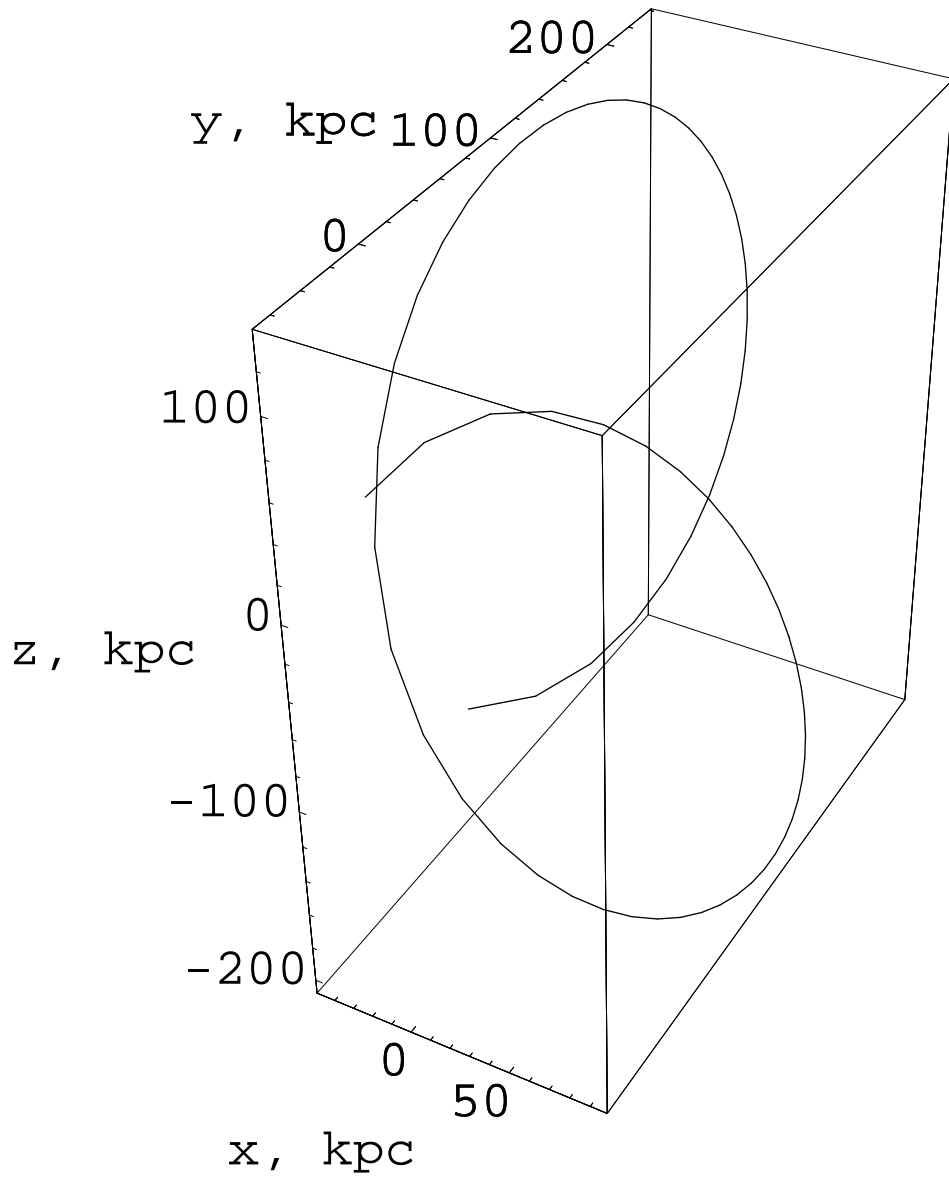


Figure 24: Numerically integrated trajectory of SMC around a mass $M = 6.5 \times 10^{10} M_{\odot}$, located at the origin, affected by the MOG acceleration of eq. (19) for the central values of the initial conditions of Table 1. The integration time span is 10 Gyr backward in time.

CDM scenario and in the modified models of gravity by MOND and MOG; at such galactocentric distances, there is no need of accurate modeling of the spatial distribution of matter, both baryonic and exotic. We tailored our analysis on the Milky Way both with respect to its electromagnetically detected baryonic mass content and the DM halo.

In the framework of Newtonian dynamics, we used an effective DM halo mass density profile able to reproduce well the observed rotation velocity curve of the Galaxy; then we used it to numerically integrate the equations of motion of fictitious and real test particles over some Gyr with different initial conditions yielding both co-planar and out-of-plane (SMC) orbital configurations. Concerning the initial velocities, we just used the values predicted by our effective DM model as representative of the real velocities.

The same initial conditions and integration intervals were also used to numerically solve the equations of motion both in MOND and MOG. Concerning MOND, we used $\mu = X$, $\mu = X/\sqrt{1+X^2}$ and $\mu = X/(1+X)$. It turns out that, contrary to our DM model, all the three MONDian forms of μ do not allow for co-planar, circular orbits yielding, instead, quite different orbital patterns. Also in the case of the out-of-plane motion of SMC, whose measured velocity is in agreement with the predictions of our effective DM model within the errors, MOND and DM yield different orbital motions. In general, the dynamics induced by $\mu = X$ and $\mu = X/\sqrt{1+X^2}$ slightly differ from that by $\mu = X/(1+X)$. MOG tend to mimics, to a certain extent, the MOND orbital scenarios.

In conclusion, our analysis shows that it is possible, in principle, to discriminate between MOND and DM at large galactocentric distances, although accurate observations are difficult to be collected there. Moreover, MOND (and MOG), with realistic initial conditions for the velocity, do not allow for co-planar, circular orbits.

References

- [1] F. Zwicky, “Die Rotverschiebung von extragalaktischen Nebeln,” *Helvetica Physica Acta*, vol. 6, pp. 110-127, 1933.
- [2] A. Bosma, “21-cm line studies of spiral galaxies. I - Observations of the galaxies NGC 5033, 3198, 5055, 2841, and 7331. II - The distribution and kinematics of neutral hydrogen in spiral galaxies of various morphological types”, *The Astronomical Journal*, vol. 86, December 1981, pp. 1791-1846, 1981.

- [3] M. Persic, P. Salucci, and F. Stel, “The universal rotation curve of spiral galaxies - I. The dark matter connection”, *Monthly Notices of the Royal Astronomical Society*, vol. 281, no. 1, pp. 27-47, 1996.
- [4] M. Persic, P. Salucci, and F. Stel, “Erratum: The universal rotation curve of spiral galaxies - I. The dark matter connection”, *Monthly Notices of the Royal Astronomical Society*, vol. 283, December 1996, p. 1102, 1996.
- [5] V. C. Rubin, W. K. Ford, N. Thonnard, and D. Burstein, “Rotational properties of 23 SB galaxies”, *The Astrophysical Journal*, vol. 261, October 15, pp. 439-456, 1982.
- [6] V. C. Rubin, “The Rotation of Spiral Galaxies”, *Science*, vol. 220, no. 4604, pp. 1339-1344, 1983.
- [7] S. Khalil and S. Muñoz, “The enigma of the dark matter”, *Contemporary Physics*, vol. 43, no. 2, pp. 51-61, 2002.
- [8] P. Salucci, and A. Borriello, “The Intriguing Distribution of Dark Matter in Galaxies”, in *Particle Physics in the New Millennium. Lecture Notes in Physics*, vol. 616, J. Trampeti and J. Wess, Eds., pp. 66-77, Springer, Berlin, 2003.
- [9] B. Famaey, and J. Binney, “Modified Newtonian dynamics in the Milky Way”, *Monthly Notices of the Royal Astronomical Society*, vol. 363, no. 2, pp. 603-608, 2005.
- [10] M. Milgrom, “A Modification of the Newtonian Dynamics as a Possible Alternative to the Hidden Mass Hypothesis”, *The Astrophysical Journal*, vol. 270, July 15, pp. 365-370, 1983a.
- [11] M. Milgrom, “A Modification of the Newtonian Dynamics - Implications for Galaxies”, *The Astrophysical Journal*, vol. 270, July 15, pp. 371-389, 1983b.
- [12] M. Milgrom, “A Modification of the Newtonian Dynamics - Implications for Galaxy Systems”, *The Astrophysical Journal*, vol. 270, July 15, pp. 384-389, 1983c.
- [13] K. G. Begeman, A. H. Broeils, and R. H. Sanders, “Extended rotation curves of spiral galaxies - Dark haloes and modified dynamics”, *Monthly Notices of the Royal Astronomical Society*, vol. 249, April 1, pp. 523-537, 1991.

- [14] J. D. Bekenstein, and M. Milgrom, “Does the Missing Mass Problem Signal the Breakdown of Newtonian Gravity?”, *The Astrophysical Journal*, vol. 286, November 1, pp. 7-14, 1984.
- [15] J. D. Bekenstein, “Relativistic gravitation theory for the modified Newtonian dynamics paradigm”, *Physical Review D*, vol. 70, no. 8, id. 083509, 2004.
- [16] J.-P. Bruneton, and G. Esposito-Farèse, “Field-theoretical formulations of MOND-like gravity”, *Physical Review D*, vol. 76, no. 12, id. 124012, 2007.
- [17] H. Zhao, “Coincidences of Dark Energy with Dark Matter: Clues for a Simple Alternative?”, *The Astrophysical Journal*, vol. 671, no. 1, pp. L1-L4, 2007.
- [18] R. H. Sanders, and S. S. McGaugh, “Modified Newtonian Dynamics as an Alternative to Dark Matter”, *Annual Review of Astronomy and Astrophysics*, vol. 40, September 2002, pp. 263-317, 2002.
- [19] J. D. Bekenstein, “The modified Newtonian dynamics - MOND and its implications for new physics”, *Contemporary Physics*, vol. 47, no. 6, pp. 387-403, 2006.
- [20] M. Milgrom, “The MOND paradigm”, Talk presented at the XIX Rencontres de Blois “Matter and energy in the Universe: from nucleosynthesis to cosmology”, May 2007, <http://arxiv.org/abs/0801.3133v2>.
- [21] M. Sereno, and Ph. Jetzer, “Dark matter versus modifications of the gravitational inverse-square law: results from planetary motion in the Solar system”, *Monthly Notices of the Royal Astronomical Society*, vol. 371, no. 2, pp. 626-632, 2006.
- [22] J. D. Bekenstein, and J. Magueijo, “Modified Newtonian dynamics habitats within the solar system”, *Physical Review D*, vol. 73, no. 10, id. 103513, 2006.
- [23] R. H. Sanders, “Solar system constraints on multifield theories of modified dynamics”, *Monthly Notices of the Royal Astronomical Society*, vol. 370, no. 3, pp. 1519-1528, 2006.
- [24] L. Iorio, “Constraining MOND with Solar System dynamics”, *Journal of Gravitational Physics*, vol. 2, no. 1, pp. 26-32, 2008.

- [25] M. Cadoni, “Letter: An Einstein-Like Theory of Gravity with a Non-Newtonian Weak-Field Limit ”, *General Relativity and Gravitation*, vol. 36, no. 12, pp. 2681-2688, 2004.
- [26] J. P. Fabris, and J. Pereira Campos, “Spiral galaxies rotation curves with a logarithmic corrected newtonian gravitational potential ”, *General Relativity and Gravitation*, vol. 41, no. 1, pp. 93-104, 2009.
- [27] S. Capozziello, V. F. Cardone, G. Lambiase, and A. Troisi, “A fluid of strings as a viable candidate for the dark side of the universe”, *International Journal of Modern Physics D*, vol. 15, no. 1, pp. 6994, 2006.
- [28] C. Frigerio-Martins, and P. Salucci, “Analysis of rotation curves in the framework of R^n gravity”, *Monthly Notices of the Royal Astronomical Society*, vol. 381, no. 8, pp. 1103-1108, 2007.
- [29] J. W. Moffat, and V. T. Toth, “Testing modified gravity with globular cluster velocity dispersions”, *The Astrophysical Journal*, vol. 680, no. 2, pp. 1158-1161, 2008.
- [30] B. Famaey, J.-Ph. Bruneton, and H. Zhao, “Escaping from modified Newtonian dynamics”, *Monthly Notices of the Royal Astronomical Society: Letters*, vol. 377, no. 1, pp. L79-L82, 2007.
- [31] H. Haghi, S. Rahvar, and A. Hasani-Zonooz, “The Magellanic Stream in Modified Newtonian Dynamics”, *The Astrophysical Journal*, vol. 652, no. 1, pp. 354-361, 2006.
- [32] C. Llinares, A. Knebe, and H. Zhao, “Cosmological structure formation under MOND: a new numerical solver for Poisson’s equation”, *Monthly Notices of the Royal Astronomical Society*, vol. 391, no. 4, pp. 1778-1790, 2008.
- [33] F. Tiret, and O. Combes, “Evolution of spiral galaxies in modified gravity”, *Astronomy and Astrophysics*, vol. 464, no. 2, pp. 517-528, 2007.
- [34] F. Tiret, and O. Combes, “Evolution of spiral galaxies in modified gravity. II. Gas dynamics”, *Astronomy and Astrophysics*, vol. 483, no. 3, pp. 719-726, 2008.
- [35] M. Malekjani, S. Rahvar, and H. Haghi, “Spherical Collapse in Modified Newtonian Dynamics (MOND)”, *The Astrophysical Journal*, at press, 2009.

- [36] S. McGaugh, “Milky Way Mass Models and MOND”, *The Astrophysical Journal*, vol. 683, no. 1, pp. 137-148, 2008.
- [37] J. I. Read, and B. Moore, “Tidal streams in a MOND potential: constraints from Sagittarius”, *Monthly Notices of the Royal Astronomical Society*, vol. 361, no. 3, pp. 971-976, 2005.
- [38] C. Nipoti, P. Londrillo, H. S. Zhao, and L. Ciotti, “Vertical dynamics of disc galaxies in modified Newtonian dynamics”, *Monthly Notices of the Royal Astronomical Society*, vol. 379, no. 2, pp. 597-604, 2007.
- [39] M. Milgrom, “Modified Newtonian Dynamics Mass-to-Light Ratios for Galaxy Groups”, *The Astrophysical Journal*, vol. 577, no. 2, pp. L75-L77, 2002.
- [40] X. Wu, H. Zhao, B. Famaey, G. Gentile, O. Tiret, F. Combes, G.W. Angus, and A.C. Robin, “Loss of Mass and Stability of Galaxies in Modified Newtonian Dynamics”, *The Astrophysical Journal*, vol. 665, no. 2, pp. L101-L104, 2007.
- [41] X. Wu, B. Famaey, G. Gentile, H. Perets, and H.-S. Zhao, “Milky Way potentials in CDM and MOND. Is the Large Magellanic Cloud on a bound orbit?”, *Monthly Notices of the Royal Astronomical Society*, vol. 386, no. 4, pp. 2199-2208, 2008.
- [42] J. W. Moffat, and V. T. Toth, “Fundamental parameter-free solutions in modified gravity”, <http://arxiv.org/abs/0712.1796v4>.
- [43] L. Iorio, “Putting Yukawa-Like Modified Gravity (MOG) on the Test in the Solar System ”, *Scholarly Research Exchange*, vol. 2008, id 238385, 2008.